lipidology

MDPI

Article

PPARγ Deficiency in SZ95 Sebocytes Elicits Redox Stress and Impairs the Sequestosome/Autophagy-Mediated Clearance of Oxidized Lipids

Alexandra Stiegler [1], Michaela Schirato [1,2], Ionela-Mariana Nagelreiter [1,2,3], Christina Bauer [1,2], Sarah Jelleschitz [1,2], Christopher Kremslehner [1,2], Christos C. Zouboulis [4], Dóra Kovács [5], Kinga Lénárt [5], Miriam Maiellaro [6], Emanuela Camera [6], Dániel Törőcsik [5,7] and Florian Gruber [1,2,*]

1 Department of Dermatology, Medical University of Vienna, Spitalgasse 23, 1090 Vienna, Austria; alexandra.stiegler@muv.ac.at (A.S.); michaela.schirato@muv.ac.at (M.S.); ionela-mariana.nagelreiter@muv.ac.at (I.-M.N.); christina.bauer@muv.ac.at (C.B.); sarah.jelleschitz@muv.ac.at (S.J.); christopher.kremslehner@muv.ac.at (C.K.)
2 Christian Doppler Lab for Skin Multimodal Imaging of Aging and Senescence (CDL SKINMAGINE), 1090 Vienna, Austria
3 Center for Brain Research, Medical University of Vienna, Spitalgasse 4, 1090 Vienna, Austria
4 Department of Dermatology, Venereology and Immunology, Universitaetsklinikum Ruppin-Brandenburg, Brandenburg Medical School Theodor Fontane and Faculty of Health Sciences Brandenburg, 16816 Neuruppin, Germany; christos.zouboulis@mhb-fontane.de
5 Department of Dermatology, University of Debrecen, 4032 Debrecen, Hungary; kovacs.dora@med.unideb.hu (D.K.); kinga.lenart@med.unideb.hu (K.L.); torocsik.daniel@med.unideb.hu (D.T.)
6 Laboratory of Cutaneous Physiopathology, Integrated Centre of Metabolomics Research, San Gallicano Dermatological Institute IRCCS, 00144 Rome, Italy; miriam.maiellaro@ifo.it (M.M.); emanuela.camera@ifo.it (E.C.)
7 HUN-REN-UD Allergology Research Group, 4032 Debrecen, Hungary
* Correspondence: florian.gruber@meduniwien.ac.at

Abstract

Background/Objectives: Sebocytes, the primary cell type in sebaceous glands (SGs), produce a lipid mixture called sebum that is released onto the skin surface and is required for skin homeostasis. The lipid receptor Peroxisome Proliferator-Activated Receptor gamma (PPARγ) regulates sebocyte proliferation and lipid synthesis and is involved in acne development. As inhibition of PPARγ has been shown to reduce insulin-induced lipogenesis and *Akt/mTOR* signalling in SZ95 sebocytes, we here investigated the effects of PPARγ deletion on lipid homeostasis and autophagic stress responses and how the secretomes affect dermal fibroblasts. **Methods:** SZ95 sebocytes wildtype (WT) and PPARγ knockout (KO) were shifted to low serum and EGF-deficient conditions permissive for autophagy. Untargeted and targeted HPLC-MS/MS analyses were used to analyze native and oxidized lipids, respectively. Protein levels of LC3I/II and p62 were assessed using immunoblots and immunofluorescence microscopy to investigate the autophagic flux. Dermal fibroblasts were exposed to conditioned media. **Results:** In low serum culture media, KO SZ95 sebocytes displayed significantly altered levels of 23 lipid classes. We observed a significant increase in ether-linked fatty acids as components of complex lipids and detected elevated levels of phospholipid hydroperoxides and aldehydolipids in the KO sebocytes. KO SZ95 sebocytes failed to show the typical responses to lipoxidative stress, such as elevated p62 crosslinking or inclusion body formation, and had reduced LC3II/I ratios as compared to WT cells. PPARγ KO conditioned media promoted a trend towards an inflammatory fibroblast phenotype. **Conclusions:** These findings suggest that PPARγ in sebocytes may alter the lipidome, elevate redox stress, and affect the autophagic machinery, which could cause accumulation of oxidized lipids and other potentially harmful compounds in sebocytes.

Academic Editors: Maria Pia Adorni and Bianca Papotti

Received: 24 March 2026
Revised: 5 May 2026
Accepted: 11 May 2026
Published: 20 May 2026

Keywords: PPARγ; sebocytes; lipid synthesis; autophagy

1. Introduction

The sebaceous gland (SG) is a lipid-producing skin appendage, forming the pilosebaceous unit together with the hair follicle. Sebocytes originate from epithelial stem cells and produce and metabolize lipids, which are released through holocrine secretion as the cells undergo terminal differentiation [1,2]. Although the composition of sebum is species-specific, sebum lipids in humans provide photoprotection, antimicrobial activity, and delivery of fat-soluble antioxidants and anti-inflammatory compounds to hair and the skin surface [3].

During holocrine secretion, autophagy is activated in sebocytes and is important for lipogenesis [4], while we had shown that it is also required for lipid redox homeostasis, sebocyte nutrition, and holocrine secretion [5–7]. Importantly, oxidized phospholipids can be cleared by autophagy to restore homeostasis after oxidative stress, such as UV radiation [8,9]. Defective autophagy in a mouse model caused SG hyperplasia and a changed lipid profile [10], while in murine preputial glands, a functionally similar sebocyte-dominated organ, autophagy deficiency resulted in the disruption of gland homeostasis and aberrant holocrine secretion [7].

The transcription factor Peroxisome Proliferator-Activated Receptor gamma (PPARγ) is a regulator of lipid metabolism and also of differentiation in sebocytes [11,12]. The influence of PPARγ on the production of lipids that are precursors of inflammatory mediators suggests that it plays a role in inflammatory sebaceous disorders such as acne [11]. We here also explore how fibroblasts, which surround the pilosebaceous unit, respond to the secretome of sebocytes with and without PPARγ. An immunomodulatory role of fibroblasts (which in all likelihood, are exposed to inflammatory signals from sebocytes in vivo) has only recently been reported [13]. On the other hand, immunomodulatory (oxidized) lipids are ligands for PPARγ [14], which may be important in inflammatory events [15] that involve SGs. Regarding the role of PPARγ in autophagy, previous studies reported its positive regulatory effect through the inhibition of mTOR signalling, which plays a central role in sebocyte differentiation [16,17].

This study aimed to further address how PPARγ is involved in sebocyte fate and autophagy initiation [4,18]. In this study, we used the SZ95 human sebocyte cell line [19] and the CRISPR/Cas9 method to delete PPARγ [20] to elucidate the total lipidome composition in PPARγ-deficient (KO) SZ95 sebocytes under conditions of low serum and low epidermal growth factor (EGF) that favour autophagy. Using bioinformatic methods, we evaluated the biological impact of the detected changes in the lipidome. Additionally, we examined the autophagic flux following the inhibition and induction of autophagy, as well as induced oxidative stress.

2. Materials and Methods

2.1. Sebocyte Cell Culture

Immortalized human SZ95 sebocytes [19] were cultured in Dulbecco's Modified Eagle's Medium (DMEM)/Nutrient Mixture F-12 Ham (F-12) (Sigma-Aldrich, St. Louis, MO, USA) supplemented with 10% fetal bovine serum (FBS) heat inactivated (Sigma-Aldrich), 1 mM $CaCl_2$, 2.5 mM Alanyl-Glutamine (Ala-Gln, 200 mM; Sigma-Aldrich), 5 ng human EGF (Sigma-Aldrich) and 1% penicillin-streptomycin (Gibco, Thermo Fisher, Waltham, MA, USA). SZ95 sebocytes with a PPARγ KO were generated by CRISPR gene editing, and

the knockdown was confirmed by immunoblotting (Appendix A Figure A1). The further characterization of the knockdown is presented in [20].

For all experiments, the sebocytes were shifted to low serum conditions, and the treatments were done in DMEM/F-12 (Sigma-Aldrich) supplemented with 1% FBS heat-inactivated (Sigma-Aldrich), 1 mM $CaCl_2$, 2.5 mM Ala-Gln (200 mM; Sigma-Aldrich), and 1% penicillin-streptomycin (Gibco, Thermo Fisher).

2.2. Fibroblast Cell Culture

The collection of skin samples used for cell isolation in this study was approved by the Ethics Committee of the Medical University of Vienna (approval number 1969/2021), and written informed consent was obtained from all participants. Primary human fibroblasts (hFB) were cultured in DMEM/F-12 supplemented with GlutaMAX (Gibco, Thermo Fisher), 10% FBS heat-inactivated (Sigma-Aldrich), and 1% penicillin-streptomycin (Gibco, Thermo Fisher).

To generate the sebocyte conditioned media, the SZ95 sebocytes were incubated for 24 h in the sebocyte experiment medium, which was subsequently collected in a Falcon™ 15 mL Conical Centrifuge Tube (Thermo Fisher) and centrifuged at 3750 RPM for 5 min, and afterwards applied to the fibroblasts.

2.3. Lipid Isolation and Analysis

Wildtype (WT) and KO SZ95 sebocytes were harvested after 24 h of treatment with medium containing reduced FBS. Sebocytes were washed with PBS (Gibco, Thermo Fisher) containing BHT (0.01%) (Sigma-Aldrich). Sebocytes (2×10^6 cells/sample) were scraped on ice in 1 mL of methanol/BHT (0.01%) for lipid extraction.

Lipid isolation from SZ95 cells was performed using liquid–liquid extraction, as recently described in refs. [21,22]. In summary, the experiment was performed on technical triplicates, as a cell line was used during the collection of materials. Each step was performed on ice. A total of 100 ng of internal standard (1,2-dimyristoyl-*sn*-glycero-3-phosphocholin [DMPC]) (Avanti Polar Lipids, Alabaster, AL, USA) was added to each sample. Meanwhile, 1 mL methanol/BHT (0.01%), 4 mL chloroform/BHT (0.01%), and 1.5 mL formic acid (0.7 M) were added to the methanol phase, and after vortexing, the lower organic phase was transferred into a new glass vial. Before continuing with the washing steps, 3 mL of the total lipid samples were dried under argon and set aside in storage at −20 °C for LC-MS/MS analysis. In total, 1 mL of the total extracted lipids was continued with washing three times with 4 mL hexan/BHT (0.01%). The washed samples had another internal standard (1,2-dinnanoyl-*sn*-glycero-3-phosphocholine [DNPC]) (Avanti Polar Lipids) added. Next, 4 mL chloroform/BHT (0.01%) and 1.5 mL formic acid were added. The bottom phase was transferred into new glass vials and afterwards dried under argon and stored at −20 °C until phospholipid HPLC MS/MS analysis.

2.4. LC-MS/MS Analysis

LC-MS/MS measurement was performed by the Metabolomics Core Facility of the EMBL, Heidelberg, Germany.

LC-MS grade water, acetonitrile, isopropanol, and methanol were obtained from Th. Geyer (Renningen, Germany). High-purity ammonium acetate, ammonium formate, ammonium hydroxide (25%, *w*:*v*), and formic acid were purchased from Merck (Darmstadt, Germany). For internal standards, a labelled lipid standard mixture (EquiSPLASH; Avanti Polar Lipids) was used at a final concentration of 0.5%.

Samples were collected and prepared as described above. Dried samples were reconstituted in isopropanol/methanol (50:50, *v*:*v*) to yield a uniform concentration of 1 million cells/100 µL. After vortexing for 30 s and subsequent centrifugations for

10 min at 15,000 *g* and 4 °C with a 5415R microcentrifuge (Eppendorf, Hamburg, Germany), extract supernatants were transferred to analytical glass vials and placed in the autosampler.

LC-MS/MS analysis was performed on a Vanquish UHPLC system coupled to an Orbitrap Exploris 240 high-resolution mass spectrometer (Thermo Fisher) in negative ESI (electrospray ionization) mode.

Chromatographic separation was carried out on an ACQUITY Premier CSH C18 column (2.1 mm × 100 mm, 1.7 µm; Waters, Milford, MA, USA) at a flow rate of 0.3 mL/min. The mobile phase consisted of water:ACN (40:60, *v*/*v*; mobile phase A) and IPA:ACN (9:1, *v*/*v*; mobile phase B), which were modified with a total buffer concentration of 10 mM ammonium acetate + 0.1% acetic acid (negative mode) and 10 mM ammonium formate + 0.1% formic acid (positive mode), respectively. The following gradient (23 min total run time including re-equilibration) was applied (min/%B): 0/15, 2.5/30, 3.2/48, 15/82, 17.5/99, 19.5/99, 20/15, 23/15. Column temperature was maintained at 65 °C, the autosampler was set to 4 °C, and the sample injection volume was 2 µL (positive mode) and 4 µL (negative mode).

Analytes were recorded via a full scan with a mass resolving power of 120,000 over a mass range from 200 to 1700 *m*/*z* (scan time: 100 ms, RF lens: 70%). To obtain MS/MS fragment spectra, data-dependent acquisition was carried out (resolving power: 15,000; scan time: 54 ms; stepped collision energies [%]: 25/35/50; cycle time: 600 ms). Ion source parameters were set to the following values: spray voltage: 3250 V/3000 V, sheath gas: 45 psi, auxiliary gas: 15 psi, sweep gas: 0 psi, ion transfer tube temperature: 300 °C, vaporizer temperature: 275 °C.

All experimental samples were measured in a randomized manner. Pooled quality control (QC) samples were prepared by mixing equal aliquots from each processed sample. Multiple QCs were injected at the beginning of the analysis in order to equilibrate the analytical system. A QC sample was analyzed after every 5th experimental sample to monitor instrument performance throughout the sequence. For the determination of background signals and subsequent background subtraction, an additional processed blank sample was recorded. Data was processed using MS DIAL [23], and raw peak intensity data was normalized via total ion count of all detected analytes [24]. Feature identification was based on accurate mass, isotope pattern, MS/MS fragment scoring, retention time, and intra-class elution pattern matching [25].

2.5. Phospholipid HPLC MS/MS

The FTC-Forensic Toxicological Laboratory, Vienna, carried out the mass spectrometry of purified phospholipids as described in [22]. To summarize, previously dried samples were reconstituted in 85% aqueous methanol supplemented with 5 mM ammonium formate and 0.1% formic acid. Meanwhile, 10 µL aliquots were transferred into a core–shell type C18 column (Kinetex 2.6 µm, 50 mm 3.0 mm ID; Phenomenex, Torrance, CA, USA) and kept at 20 °C. A 1200 series HPLC system (Agilent Technologies, Waldbronn, Germany) coupled to a 4000 QTrap triple quodupole linear ion trap hybrid mass spectrometer system equipped with a Turbo V electrospray ion source (Applied Biosystems, Foster City, CA, USA) was used. Lipid species were detected in positive ion mode by selected reaction monitoring of 99 MS/MS transitions using a PC-specific product ion (*m*/*z* 184), which corresponds to the cleaved phosphocholine residue. Analyst software, version 1.6 (Applied Biosystems), was used for data acquisition and instrument control. Individual values were normalized to the intrinsic DPPC.

2.6. Pathway and Enrichment Analysis

BioPAN (https://www.lipidmaps.org/biopan/, accessed on 11 November 2024) [26] was used to complete the pathway analysis and visualize the key pathways responsible for the lipid differences found in the data. BioPAN generates a list of the most active and most suppressed pathways by Z-score, with a significance level of $p < 0.05$, which corresponds to $Z > 1.645$.

Lipid ontology (LION, http://lipidontology.com/, accessed on 11 November 2024) enrichment analysis was performed to compare the lipidomic fingerprint of SZ95 WT and KO sebocytes [27,28]. LION/web was used to associate molecular lipid species with lipid classification, function, and distribution within the cellular components. Enrichment analysis was performed using the ranking mode as described by [27,28]. The analysis parameters set SZ95 WT sebocytes as the control condition and SZ95 KO sebocytes as the condition of interest. P-values calculated by LION/web were adjusted for multiple testing [29].

2.7. Lipid Oxidation Assay (Fluorescence WL Shift-Based)

BODIPY C11 581/591 undecanoic acid (Invitrogen, Thermo Fisher) was used to visualize lipid peroxidation as per the manufacturer's specifications. SZ95 sebocytes were seeded into 4-chamber polystyrene vessel tissue culture-treated glass slides (Falcon, Corning, Tewksbury, MA, USA) and cultured for 24 h. The sebocytes were treated with 2 µM BODIPY C11 and 1 µM Höchst (33342, Invitrogen, Thermo Fisher) in culture medium in darkness for 30 min at 37 °C with a 5% CO_2 atmosphere. The Lipid Peroxidation Sensor has a fluorescence emission peak at red ~590 nm when localized to the membranes of living cells. Oxidation of the polyunsaturated butadienyl portion of the fatty acid analogue leads to a shift in the fluorescence emission peak to green ~510 nm. For both SZ95 WT and KO sebocytes, nine sites were photographed, and these fields of view were analyzed using Fiji (ImageJ (1.54k, 2024), National Institutes of Health, Bethesda, MD, USA). Staining intensity was measured in a virtual cross-section through the cells, which was created with the "segmented line" tool. The "Plot Profile" of the cross-section was generated, and the data was transferred into Microsoft Excel. Log2 fold change of the ratio of oxidized (green) to non-oxidized (red) per pixel was calculated as described in [30].

2.8. ROS Detection Assay

The CellROX Green Reagent (Invitrogen, Thermo Fisher) was used to measure intracellular reactive oxygen species (ROS) formation in accordance with the manufacturer's specifications. SZ95 sebocytes were seeded into a 4-chamber polystyrene vessel tissue culture-treated glass slides (Falcon, Corning) and cultured for 24 h. Next, the sebocytes were incubated with 5 µM CellROX for 30 min at 37 °C with a 5% CO_2 atmosphere. The cells were fixated with 3.7% formaldehyde (SAV Liquid Production GmbH, Flintsbach am Inn, Germany) for 20 min at room temperature. Afterwards, cell nuclei were stained with 1 µM Höchst (33342, Invitrogen, Thermo Fisher). The staining was examined with an LSM700 inverse point scanning confocal microscope (Zeiss, Oberkochen, Germany). Upon oxidation by ROS and binding to DNA, CellROX displayed a bright green photostable fluorescence signal with absorption/emission maxima of 485/520 nm. For both SZ95 WT and KO sebocytes, nine sites were photographed, and these fields of view were analyzed using Fiji (ImageJ, National Institutes of Health). Staining intensity was measured in a virtual cross-section through the cells, which was created with the "segmented line" tool. The "Plot Profile" of the cross-section was generated, and the data was transferred into Microsoft Excel. Mean intensity per stained pixel was calculated as described in [30].

2.9. Induction and Inhibition of Autophagy

For the induction of autophagy in sebocytes, we used the reference drug rapamycin (RAPA, 10 mM Merck), diluted to a final concentration of 0.5 µM, and oxidized phospholipids (OxPAPC) [8], diluted to a final concentration of 25 µg/mL. For inhibition of autophagy, we used 3-Methyladenine (3MA, stock 50 mM, Merck), diluted to a final concentration of 10 mM.

SZ95 WT and KO sebocytes were seeded at 5000 cells per cm^2 into six-well plates. Upon reaching confluency of 50%, treatment was started. Each well was treated with 3 mL medium. 1-Palmitoyl-2-arachidonyl-sn-glycero-3-phosphorylcholine (PAPC, Avanti Polar Lipids) was prepared in 600 µg/mL stocks by drying the lipid with argon onto the wall of glass vials (4 mL, VWR Avantor, Radnor, PA, USA) and oxidizing for five days with compressed air in darkness [31]. All reagents were diluted in Dulbecco's Modified Eagle's Medium/Nutrient Mixture F-12 Ham (Sigma-Aldrich) supplemented with 1% fetal bovine serum (FBS, heat-inactivated, Sigma-Aldrich), 1 mM $CaCl_2$, 2.5 mM Alanyl-Glutamine (200 mM, Sigma-Aldrich), and 1% penicillin-streptomycin (Gibco, Thermo Fisher). When 3MA treatment was combined with either OxPAPC or rapamycin, the 3MA was diluted to a concentration of 20 mM, of which 1.5 mL was added to each well for 2 h. Afterwards, the reagents for the combined treatment were added, and the final concentration as described above was achieved for the treatment duration. Sebocytes were harvested after 4 h or 24 h to investigate early-stage autophagy and late-stage autophagy, respectively.

2.10. Western Blotting

SZ95 WT and KO sebocytes were collected after 4 h and 24 h of treatment. Harvesting and immunoblotting were performed as described in [21].

Proteins were harvested with the 4× Laemmli Sample Lysis Buffer (Bio-Rad, Hercules, CA, USA) combined with protease (Complete tablets, Roche Diagnostics GmbH, Rotkreuz, Switzerland) and phosphatase (Thermo Fisher Scientific) inhibitors. A sodium dodecyl sulfate polyacrylamide gel electrophoresis (4–12%, Bio-Rad) was performed in a Criterion Electrophoresis system (Bio-Rad). Cell lysates were run at 200 Volt for 35 min to ensure the required degree of separation. Next, the proteins were blotted on a nitrocellulose membrane (Bio-Rad) using the Trans-Blot Turbo Transfer System (Bio-Rad). After blotting, the membrane was blocked with 5% dry milk in PBS with 0.1% Tween20 for 1 h at room temperature. Overnight antibody incubation at 4 °C was done with LC3B (GTX82986, 1:2000, GeneTex, Irvine, CA, USA), p62 (PM045, 1:1000, MBL, Tokyo, Japan) or βTubulin (ab6046, 1:5000, Abcam, Cambridge, UK). The next day, the membrane was incubated with the corresponding secondary antibody, rabbit IgG-HRP (BioRad, 1706515, 1:10,000) at room temperature for 1 h. The membrane was washed and developed with Super Signal West Dura Extended Duration Substrate (Thermo Fisher). Protein concentration was measured using Image Lab 6.1 (Bio-Rad Laboratories, Hercules, CA, USA). Target protein concentration was normalized to βTubulin concentration. The ratio of LC3 II/I was calculated from these values. The total amount of LC3 was calculated by adding the concentration of LC3 I and LC3 II and then normalized to the WT control. p62 and high molecular weight p62 (HMW p62) was normalized to the WT control.

2.11. Immunofluorescence

SZ95 sebocytes were seeded into a 4-chamber polystyrene vessel tissue culture-treated glass slides (Falcon, Corning) and cultured for 24 h. Cells were treated for 48 h as described above to induce/inhibit autophagy. Afterwards, cells were washed with PBS and fixed with Methanol at −20 °C for 10 min and stained for anti-p62 (SQSTM1) pAB (PM045, 1:1000; MBL) overnight at 4 °C. Cell nuclei were stained with 1 µM Höchst (33342, Invitrogen,

Thermo Fisher). The staining was examined with an LSM700 inverse point scanning confocal microscope (Zeiss).

2.12. RNA Extraction

The TRIzol Reagent (Invitrogen, Thermo Fisher) was used for total RNA extraction. The RNeasy® MiniElute® Cleanup Kit (Qiagen GmbH, Hilden, Germany) was used to elute extracted RNA before the samples were processed during the bulk RNA sequencing.

2.13. RNA Sequencing and Data Analysis

RNA sequencing of hFB exposed to supernatant harvested from SZ95 WT and KO sebocytes for 24 h was done at the Core Facility Genomics, Medical University of Vienna.

Sequencing libraries from total RNA were prepared at the Core Facility Genomics, Medical University of Vienna, using the QuantSeq 3′ FWD protocol version 2 with unique dual indices (Lexogen, Vienna, Austria), following the low-input branch of the protocol. In total, 18 PCR cycles were used for library prep, as determined by qPCR according to the library prep manual. Libraries were QC-checked on a Bioanalyzer 2100 (Agilent Technologies) using a High Sensitivity DNA Kit for correct insert size and quantified using Qubit dsDNA HS Assay (Invitrogen, Thermo Fisher). Pooled libraries were sequenced on a NextSeq500 instrument (Illumina, San Diego, CA, USA) in 1 × 75 bp single-end sequencing mode.

On average, 7 million reads per sample were generated.

Reads in fastq format were generated using the Illumina bcl2fastq command line tool (v2.19.1.403). Reads were trimmed and filtered using cutadapt [32] version 2.8 to trim polyA tails, remove reads with N's, and trim bases with a quality of less than 30 from the 3′ ends of the reads. On average, 5 million reads were left after this procedure.

Trimmed reads in fastq format were aligned to the human reference genome version GRCh38 [33] with Gencode 29 annotations [34] using the STAR aligner [35] version 2.6.1a in 2-pass mode. Raw reads per gene were counted by STAR. Differential gene expression was calculated using DESeq2 [36] version 1.22.2.

Data was visualized using VolcaNoseR (https://huygens.science.uva.nl/VolcaNoseR/, accessed on 5 November 2025). To reduce file size, genes fulfilling the criteria padj == NA, log2FoldChange == 0 and/or GeneType != protein_coding were removed. For the visualization, log2FoldChange was blotted on the X-axis and minus_log10_padj was blotted on the Y-axis. The FoldChange threshold of 1.8 and the Significance threshold of 2 were chosen [37].

2.14. Gene Pathway Analysis

Regulated genes were analyzed with the software QIAGEN's Ingenuity® Pathway Analysis (2025 fall release, IPA®, QIAGEN, Redwood City, CA, USA, https://digitalinsights.qiagen.com/, accessed on 6 November 2025), which allowed prediction of activated signalling pathways and upstream regulatory events that were likely to cause the observed gene expression changes. Heatmaps and activation z-scores were calculated within the IPA software package and modified for better presentation as recently described [9].

2.15. Quantitative PCR Analysis

The iScript cDNA Synthesis Kit (Bio-Rad Laboratories) was used for reverse transcription of RNA into cDNA. The LightCycler 480 SYBR Green I Master Kit (Roche Diagnostics GmbH) was used for quantitative real-time PCR (qPCR) as described before [38]. The analysis was conducted on a Thermal Cycler CFX96 Real-Time System (Bio-Rad Laboratories). The model of Pfaffl et al. [39] was used for relative quantification, and the

expression of the target genes listed in Table 1 was normalized to the housekeeping gene. Beta-2-microglobulin (B2M) was used as a housekeeping gene.

Table 1. Primer sequences used for RT-qPCR.

Target Gene	Primer Sequence
B2M	Forward: GGGATCGAGACATGTAAGCAG
Beta-2-Microglobulin	Reverse: GAGCTACCTGTGGAGCAACC
FADS1	Forward: TCCTCTCTGTGGAGCTTGGG
Fatty Acid Desaturase 1	Reverse: GTCCACCCACTTCTTTCGCT
FADS2	Forward: GGTTCAGTAGCCAGCTGACA
Fatty Acid Desaturase 2	Reverse: GTAGCGGCTTCTCCTGGTAT
PTDSS2	Forward: TTCCAGACCTCATCCAGCTTAC
Phosphatidylserine Synthase 2	Reverse: CCCGTAGTCTCTCTCTGGCA
SGMS1	Forward: TCAACTGTTCTCCGAAGCTTTT
Sphingomyelin Synthase 1	Reverse: GTGATACCACCAGAGTCGCC
ELOVL5	Forward: CCACCGGTGTCTCCTTCTAC
ELOVL Fatty Acid Elongase 5	Reverse: TTGAAAACCTTTTAGCCCAAGG
SMPD1	Forward: CTCCCGCTGGCTCTATGAAG
Sphingomyelin Phosphodiesterase 1	Reverse: GAGCCAGAAGTTCTCACGGG
PEMT	Forward: GGTAACGAACAGCTCGGTGG
Phosphatidylethanolamine N-Methyltransferase	Reverse: TCCCATCGTGCAACCACATT
DGAT2	Forward: AGGTCCAAGGTGGAAAAGCA
Diacylglycerol O-Acyltransferase 2	Reverse: TGACCTCCTGCCACCTTTCT
MBOAT1	Forward: TGCATCTTTTTGTGCTGGTGT
Membrane Bound Glycerophopholipid O-Acyltransferase 1	Reverse: TGACAATCATCAGAGGCCCAG
IL-1beta	Forward: CGATGCACCTGTACGATCAC
Interleukin 1 Beta	Reverse: TCTTTCAACACGCAGGACAG
IL-8	Forward: CTCTTGGCAGCCTTCCTGATT
C-X-C Motif Chemokine Ligand 8	Reverse: TATGCACTGACATCTAAGTTCTTTAGCA
PTGS2	Forward: GCCATGGGGTGGACTTAAA
Prostaglandin-Endoperoxide Synthase 2	Reverse: CAGCAAACCGTAGATGCTCA
Col1A1	Forward: GTGCTAAAGGTGCCAATGGT
Collagen Type I Alpha 1 Chain	Reverse: CTCCTCGCTTTCCTCCTCT
Col3A1	Forward: CTGGTGCTCCTGGACAGAAT
Collagen Type III Alpha 1 Chain	Reverse: GGGGTCCTGGGTTACCATTA

2.16. Statistical Analysis

For all statistical analyses, except for the fatty acyl chain length, and graphical representation of the data, GraphPad Prism 8.4.3 (GraphPad Software, Boston, MA, USA) was used. To calculate statistical outliers, Grubbs' test with alpha = 0.05 (Outlier Calculator, GraphPad Software) was utilized. For calculating statistical significance, *t*-Test, one-way ANOVA, and two-way ANOVA were used. Statistical significance was indicated by an asterisk with * $p < 0.05$, ** $p < 0.01$, *** $p < 0.005$, **** $p < 0.001$.

For statistical analysis of the fatty acyl chain length of the data generated by the LC MS/MS analysis, a code was written in MATLAB (R2024a, Statistics and Machine Learning Toolbox V 24.1, MathWorks, Natick, MA, USA). For statistical analysis, the Wilcoxon Rank-Sum test, which is equivalent to the Mann–Whitney U-test, was used [40]. Boxplots were generated with the Add-On daviolinplot (V 3.2.7) [41]. Significance bars were generated by the Add-On raacampbell/sigstar (V 1.76.01.1) [42].

3. Results

3.1. Deletion of PPARγ Increased the Level of Ether-Linked Complex Lipids in SZ95 Sebocytes

Previous studies showed that activation of PPARγ increased neutral lipid levels in SZ95 sebocytes when cells were cultured in a medium containing 10% FBS and EGF [12]. In the present study, SZ95 sebocytes were shifted to a medium with reduced FBS levels (1%) and no EGF, given that FBS and EGF inhibit autophagy [43].

Using an untargeted LC-MS analysis to identify 837 lipid species within 37 lipid classes in sebocytes grown under low serum, EGF-free conditions, significant changes in the percentage of total lipids were observed in 23 out of the 37 assigned lipid classes in the KO SZ95 sebocytes (Figure 1A). KO sebocytes contained significantly lower levels of phosphatidylethanolamine (PE), while phosphatidylcholine (PC) and sphingomyelin (SM) levels were significantly higher. Free fatty acid (FA) levels were significantly lower in KO SZ95 sebocytes (Figure 1A,B). We identified a shift in the sum of lipids from major lipid classes with ester-linked FAs towards lipids with ether-linked FAs, particularly among phosphatidylcholine (PC) and triglycerides (TG) (Figure 1C). In contrast, phosphatidylinositol (PI), which contains ether-linked FAs, was significantly decreased. Although PIs are present at very low abundance, they are crucial for intracellular signalling.

When we analyzed the lipid composition using the web-based interface for Lipid Ontology (LION/web, www.lipidontology.com, accessed on 11 November 2024) [27,28], we identified significantly enriched LION-terms (by ranking mode) in KO cells. These included terms of lipid classes "alkyldiacylglycerols" (TG O-, 35 species) and "1-alkyl,2-acylglycerophosphocholines" (PC O-, 71 species annotated), which both contributed to the chemical term "contains ether-bond" (106 species) (Figure 2A). This was consistent with the results from the relative quantification of lipid class level. The highest enriched term referring to cellular compartments was "endosome/lysosome", defined by 102 species.

Lipids associated with the terms "triacylglycerols" and "glycerophosphoethanolamines" were underrepresented in KO cells. These also contributed to the drop of LION-signatures for "lipid droplet" and "lipid storage". Another chemical/structural association less abundant in the KO lipidome was "polyunsaturated FAs", which included more specified terms as "FAs with more than 3 double bonds" and "FAs with 3-5 double bonds". At the level of fatty acyl species, we found the most profoundly downregulated species to be "C22:6", referring to the acyl chain in free FA. At the biophysical properties' ontology level, the terms "neutral intrinsic curvature", "very high bilayer thickness", "very high transition temperature" and "very low lateral diffusion", were enriched while the terms "above average/very high lateral diffusion", "below average and very low bilayer thickness" and "below average/low transition temperature" were underrepresented (Figure 2A).

The Bioinformatics Methodology For Pathway Analysis (BioPAN) online tool [26] predicted that glycerophospholipid metabolism in KO sebocytes was shifted towards phosphatidylserine (PS) synthesis and that they subsequently hydrolysed to lyso-PS (LPS) at the expense of PC and PE. The data suggested that hydrolysis of PI was activated, as well as further hydrolysis of PC and PE. Simultaneously, *MBOAT1* suppressed their reacylation. The data predicted the activation of TG catabolism (hydrolysis), which yielded diglycerides (diacylglycerols, DG) and free FAs (Figure 2B). Regarding the sphingolipid metabolism, the analysis predicted increased synthesis of dihydrosphingomyelins (dhSM) presumptively via the transfer of a phosphocholine group from PC onto a molecule of dihydroceramide (dhCer) catalyzed by *SGMS1/2* with DG as a side product (Figure 2B).

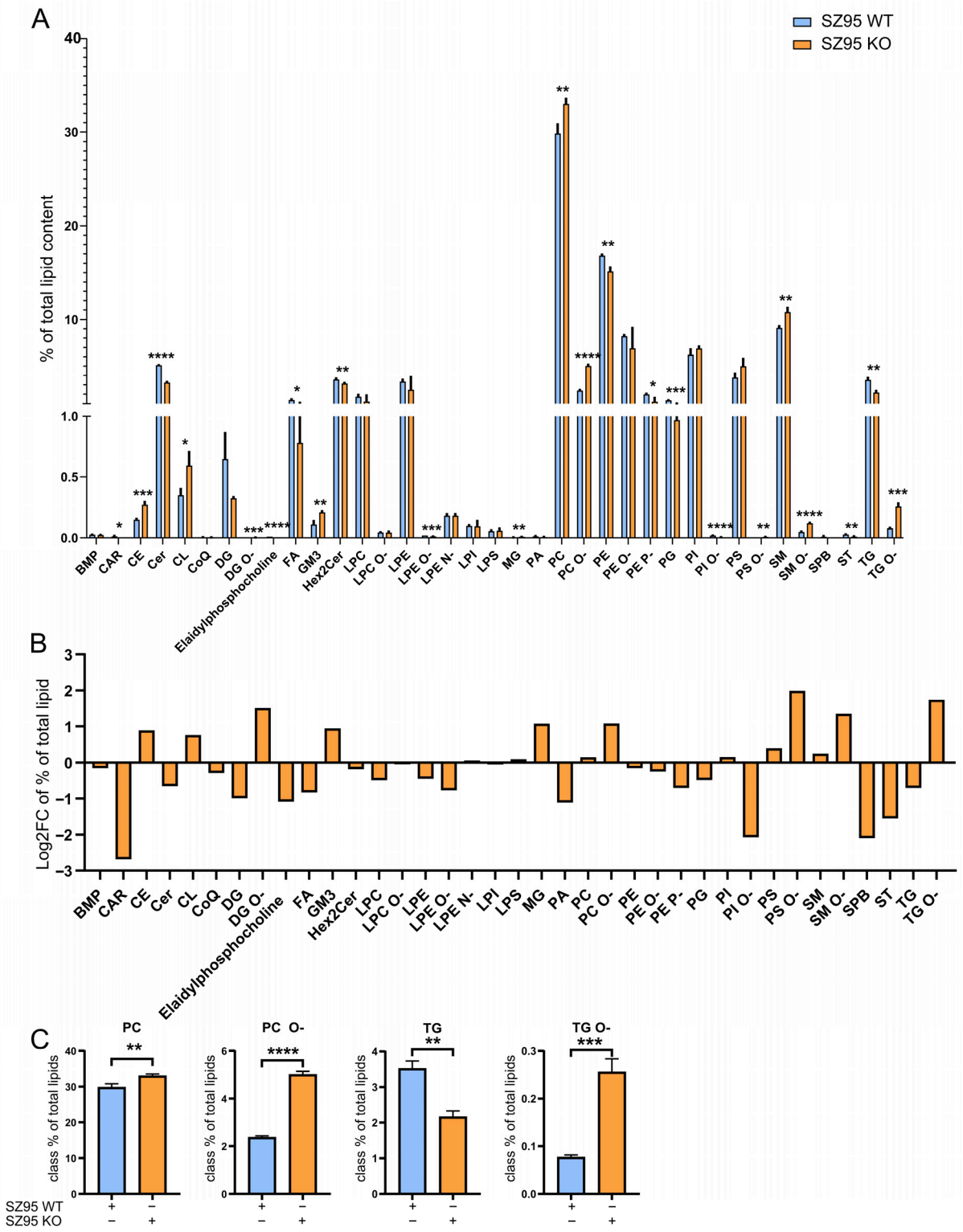

Figure 1. Untargeted lipidomic analysis of cellular lipids extracted from WT (blue) and KO (orange) SZ95 sebocytes revealed deregulation in 23 lipid classes and an accumulation of ether lipids. (**A**) Percentual distribution of total lipid content normalized to total ion current (TIC), divided into all lipid classes detected. Biological triplicates independently analyzed for each cell type; *t*-Test, * < 0.05; ** < 0.01; *** < 0.005; **** < 0.0001. (**B**) Log2 Fold Change (Log2FC) of percental distribution of total lipid content found in KO (orange) sebocytes compared to SZ95 WT (blue) sebocytes. (**C**) Percental distribution of phosphatidylcholine (PC), ether-phosphatidylcholine (PC O-), triglycerides (TG), and alkyl-triacylglycerols (TG O-) normalized to TIC. Biological triplicates independently analyzed for each cell type; *t*-Test, ** < 0.01; *** < 0.005; **** < 0.0001.

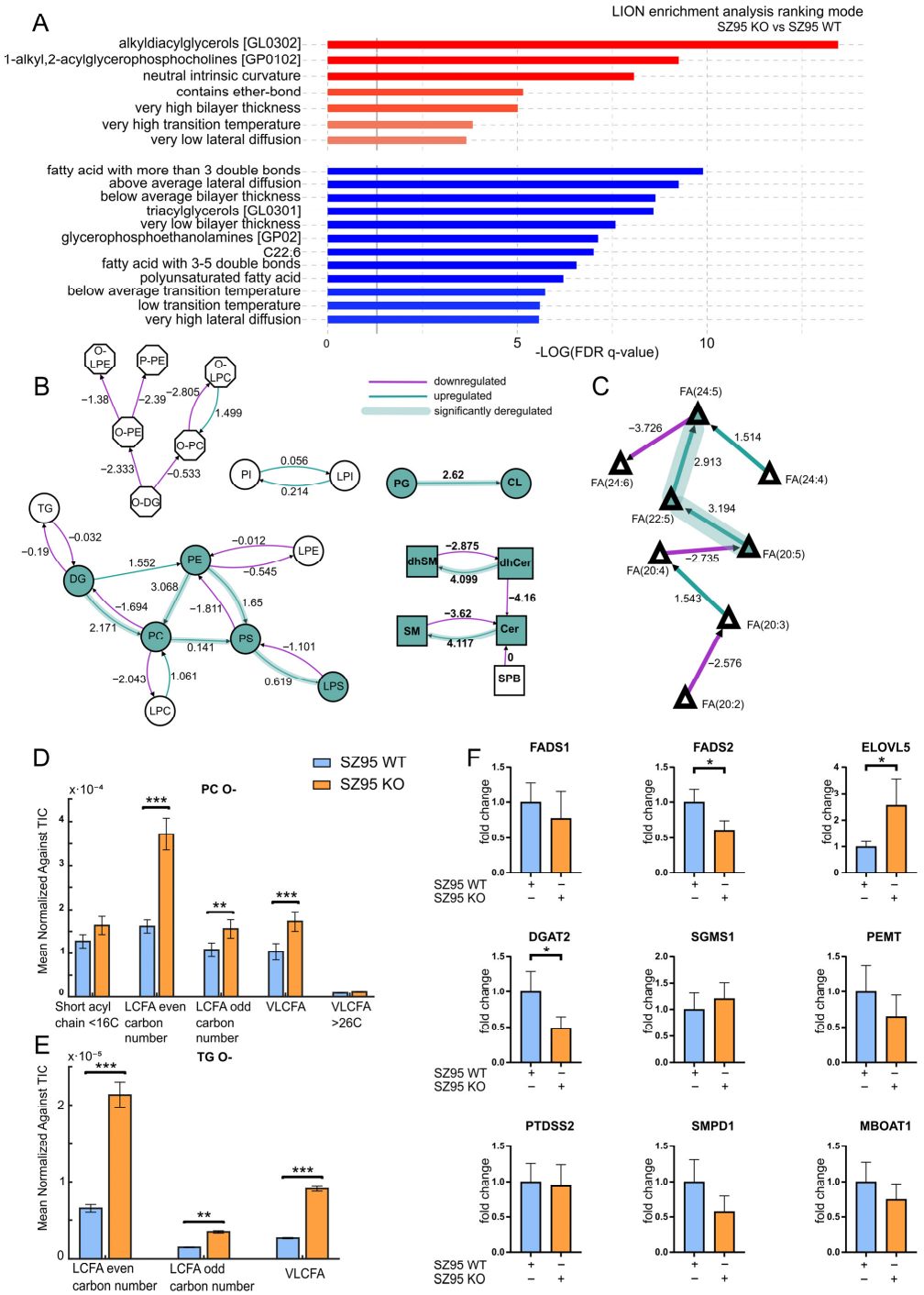

Figure 2. PPARγ KO in SZ95 sebocytes results in an elongation of FA chains. (**A**) LION enrichment analysis of KO sebocytes vs. WT sebocytes. LION terms were separated into up (red) and downregulated (blue) terms. (**B**) Activated lipid pathways suggested by BioPan in KO sebocytes compared to the wildtype. Purple lines = downregulated; blue lines = upregulated, blue overlay = significant. (**C**) Activated FA pathways in KO sebocytes compared to the WT. Purple lines = downregulated; blue lines = upregulated, blue overlay = significant. (**D**) Mean amount of FAs with short acyl chains, long-chain FAs (LCFA), and very-long-chain FAs (VLCFA) bound in ether-phosphatidylcholines (PC O-) normalized to TIC. Biological triplicates independently analyzed for each cell type; Mann–Whitney U-test, ** < 0.01, *** < 0.005. (**E**) Mean amount of LCFA and VLCFA bound in alkyl-triacylglycerols (TG O-) normalized to TIC. Biological triplicates independently analyzed for each cell type; Mann–Whitney U-test, ** < 0.01, *** < 0.005. (**F**) RNA expression levels of genes in SZ95 WT and KO sebocytes, as suggested by BioPan, are involved in the activation of different lipid pathways. Biological triplicates independently analyzed for each cell type; *t*-Test, * < 0.05.

Next, we found a shift in FA composition from long-chain FAs towards very-long and (poly-) unsaturated FAs (Figure 2C). In the overall weighted assessment of the FA side chain length, we found a trend towards an increase in short FA chains (< 16 carbons), significantly increased in long chain FAs (16–20 C) with both an even carbon number and an odd carbon number, as well as very-long chain FAs (≥22 C) in the KO sebocytes. On the lipid class level, we observed a similar increase in long-chain and very-long-chain FAs in ether-phosphatidylcholines (PC O-) and alkyl-diacylglycerols (TG O-) (Figure 2D,E).

We performed qPCR on the genes predicted to be regulated, which are involved in lipid synthesis pathways, and found that *FADS2* was significantly downregulated and *ELOVL5* was significantly upregulated in KO sebocytes. The upregulation of *ELOVL5* corroborated the finding of elongated free FAs. Another gene that was found to be significantly downregulated was *DGAT2* (Figure 2F). This corroborated our finding of higher levels of TGs than DGs in the global lipidome dataset, even though the KO sebocytes contained significantly lower levels of TGs than their WT counterparts (Figure 1A).

3.2. PPARγ Deletion Increased Oxidized Lipid Species in SZ95 Sebocytes

Previous findings of ether phospholipid deregulation, particularly in PC O- and TG O-species, indicated that they may act as regulators of mitochondrial redox control [44]. As shown above, we identified changes in ether PL levels in KO sebocytes when compared to the lipidome of WT SZ95 sebocytes. We therefore next investigated the oxidation status of selected lipids by performing a PC-targeted HPLC MS/MS redox lipidomic analysis [22].

We identified 32 lipid species present in both sebocyte genotypes, 19 of which were found to exhibit significant changes in the absence of PPARγ.

We found the initial peroxidation products of phospholipids with unsaturated FA moieties, the hydroperoxides (-OOH) [45], elevated. Specifically, the KO sebocytes displayed an elevated oxidation of *m/z* 782.7 1-Palmitoyl-2-arachidonoyl-sn-glycero-3-PC (PAPC), where especially ions tentatively identified as *m/z* (814.8) of PAPC-OOH were elevated. We also investigated advanced oxidation products of polyunsaturated FA-containing phospholipids previously described [46]. There, we found a significant increase in reactive lipid species containing aldehydes in KO sebocytes, especially in *m/z* 650.6 tentatively identified as 1-palmitoyl-2-(9-oxo)nonanoyl-*sn*-glycero-3-phosphocholine (PONPC, carbonyl), *m/z* 594.5 tentatively identified as 1-palmitoyl-2-(5-oxovaleroyl)-*sn*-glycero-3-phosphocholine (POVPC, carbonyl), and *m/z* 796.7 tentatively identified as PAPC-keto (Figure 3A).

We performed a fluorescence lipid oxidation assay using a fluorescent redox lipid sensor (BODIPY C11) to visualize and localize differences in lipid oxidation in cultured cells (Figure 3B). We found a significant decrease in the KO sebocytes in the mean value of the Log2FC of the ratio of oxidized to non-oxidized per pixel. This indicated that the KO sebocytes contained a higher ratio of oxidized to non-oxidized lipids, in line with the MS data (Figure 3C).

Since nonenzymatic lipid peroxidation is typically connected to an increase in cellular ROS, we assessed the ROS content in SZ95 KO and WT sebocytes and found a significant increase in the amount of ROS in the KOs, which is in line with the MS data where we detected increased amounts of oxidized lipid species (Figure 3D,E).

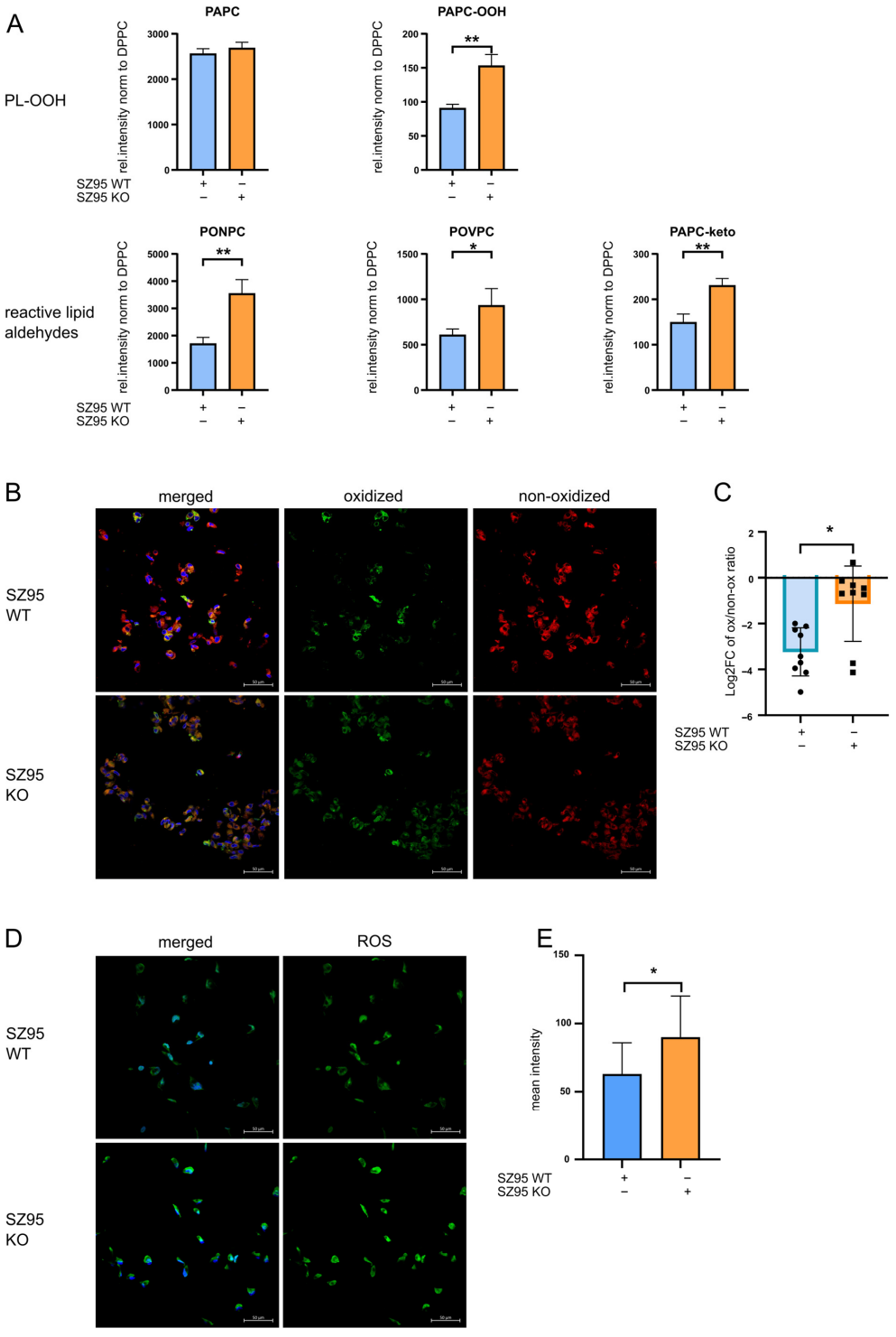

Figure 3. Oxidized phospholipids accumulate in SZ95 KO sebocytes. (**A**) Phospholipid hydroperoxides (PL-OOH), specifically PAPC-OOH were increased in KO sebocytes. Reactive lipid aldehyde species were increased in KO sebocytes. All samples were normalized to Dipalmitoylphosphatidylcholin (DPPC). Biological triplicates independently analyzed for each cell type; *t*-Test, * < 0.05; ** < 0.01. (**B**) Fluorescence lipid oxidation assay (BODIPY C11) to visualize oxidized (green) and non-oxidized (red) lipids within SZ95 WT and KO sebocytes. Scalebar indicates 50 µm. (**C**) Log2FC of the mean value ratio of pixel oxidized to non-oxidized. Nine pictures per cell type analyzed; Mann–Whitney U-test, * < 0.05. (**D**) ROS detection assay visualized ROS (green) in KO and wildtype sebocytes. Scalebar indicates 50 µm. (**E**) ROS levels depicted in mean intensity per µm. Nine pictures per cell type analyzed, *t*-Test, * < 0.05.

3.3. Knockout of PPARγ Decreases the Levels of the p62/SQSTM1 Protein in SZ95 Sebocytes

Elevated ROS and subsequent lipid peroxidation stress led to increased formation of lipid–protein adducts in human keratinocytes (KC) [47]. We had earlier demonstrated that accumulation of cross-linked p62 is indicative of this type of stress, which goes hand in hand with impairment of autophagy. Lack of autophagy also slowed down the removal of high molecular weight p62 (HMW p62) and dissolution of p62-positive inclusion bodies in KC [8].

To test for accumulation and localisation of p62 in KO and WT sebocytes, we performed an IF staining. In the WT sebocytes, rapamycin, as expected, decreased the autophagic cargo adapter p62. Inhibition of autophagy with 3MA led to its accumulation. Treatment with OxPAPC, as an external lipid oxidative stressor, led to accumulation of p62, whereas simultaneous inhibition of autophagy led to formation of p62-positive inclusion bodies. KO sebocytes, despite having higher intracellular levels of reactive oxidized lipids, did not cause accumulation of p62 in any of the treatments, and even the untreated controls showed very low levels of p62 (Figure 4).

Thus, we next performed immunoblots of protein extracts from these cells to investigate the levels of native and modified HMW p62. In the WT cells, rapamycin led to a decrease in the autophagic cargo protein p62, whereas treatment with OxPAPC led to a marked increase in the HMW form. This accumulation of the HMW form was exacerbated by the addition of the autophagy inhibitor 3MA, demonstrating that removal of HMW p62 is dependent on autophagy. The KO cells showed a clearly different pattern. The basal p62 levels were strongly reduced, and the basal and OxPAPC inducible HMW p62 accumulation was blunted (Figure 5A). Also, autophagy inhibition with 3MA did not lead to a marked accumulation of either native or HMW p62 levels, indicating that the classical macroautophagic machinery is aberrant in the KOs, with both a marked lack of the autophagy adapter p62 and reduced accumulation of its HMW form, and little response to autophagy inhibition (Appendix A Figure A2).

3.4. Deletion of PPARγ Impairs the Lipidation of LC3-I to LC3-II in SZ95 Sebocytes

A previous study showed that a KO of PPARγ in mouse prostatic epithelia resulted in the accumulation of LC3 I and II [48]. LC3, specifically its lipidation, is another marker of the autophagic flux and a rate-limiting step in autophagosome formation.

Thus, we investigated lipidation of LC3 in WT and KO sebocytes. In the SZ95 WT sebocytes, autophagy appeared to be inactive at baseline, since 3MA treatment did not lead to an accumulation of LC3 I, whereas rapamycin and 3MA combined led to an accumulation of LC3. Without treatment, the KO showed higher levels of LC3 I. Upon treatment with rapamycin, the KO cells accumulated very high levels of LC3, while the lipidation was lower after 3MA treatment (Figure 5B). This suggests that the stimulus for lipidation was still functional.

3.5. Exposure to KO Sebocyte Supernatant Deregulates the Expression of Cytokine- and Matrix-Related Genes in hFB

Previous studies suggested that oxidized lipids accumulate in chronic diseases such as atherosclerosis [31] and are able to function as inflammatory mediators [49]. Furthermore, a previous study suggested that active autophagy dampened inflammatory processes in KCs [50]. We found increased intracellular oxidized lipid species and altered autophagy, which led us to investigate the influence of the altered total secretome of KO sebocytes on human dermal cells. We exposed primary hFB to supernatant collected from either WT or KO SZ95 sebocytes for 48 h. The total RNA harvested from the cells was then subjected to bulk sequencing.

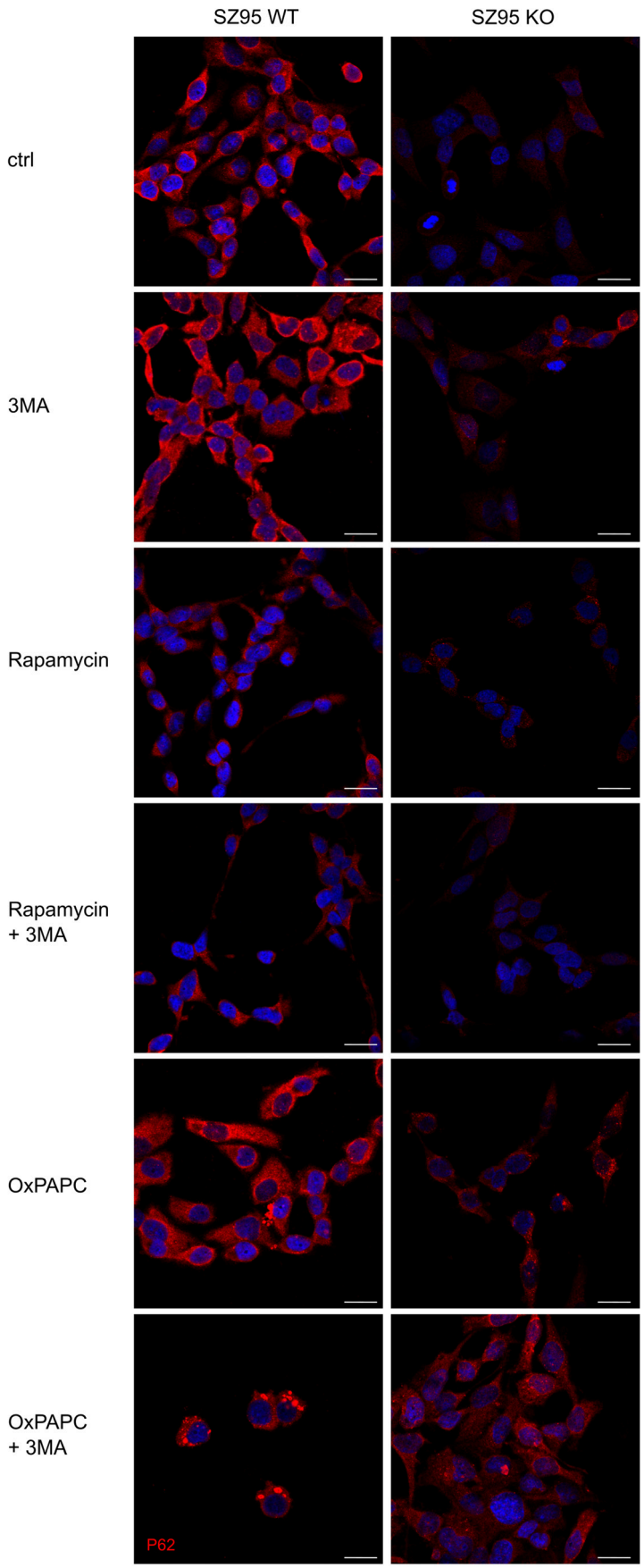

Figure 4. p62 protein expression is decreased in KO SZ95 sebocytes. Sebocytes were treated with 25 μg/mL OxPAPC, 0.5 μM rapamycin, or 10 mM 3-Methyladenine (3MA) for 48 h. IF staining with anti-p62/SQSTM1 antibody (PM045, MBL) in red. The white line indicates 20 μm.

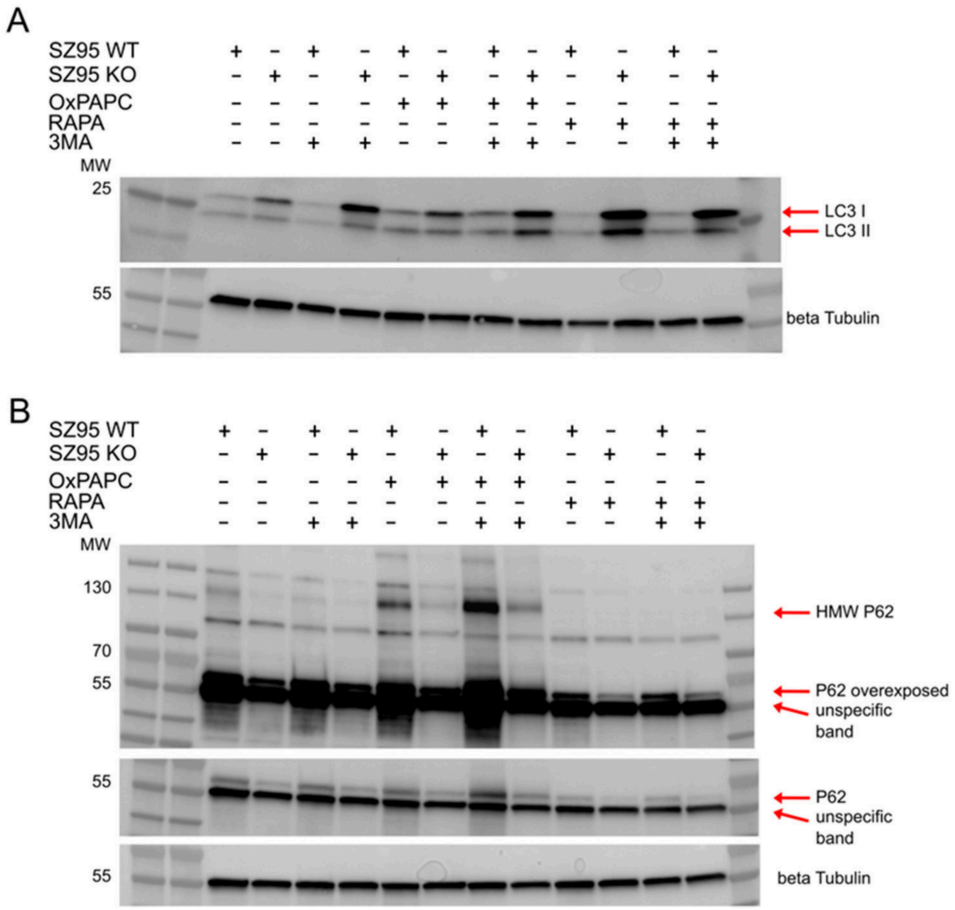

Figure 5. p62 and high molecular weight (HMW) p62 levels decreased in KO sebocytes upon induction of oxidative stress, and LC3B levels increased in KO sebocytes upon activation and inhibition of autophagy. (**A**) Western blot of SZ95 WT and KO sebocytes treated with OxPAPC, rapamycin (RAPA), or 3-Methyladenine (3MA) for 4 h. Arrows indicate the bands of LC3 I and LC3 II. Beta tubulin was used as a loading control. (**B**) Western blot of SZ95 WT and KO sebocytes treated with OxPAPC, RAPA, or 3MA for 24 h. Arrows indicate the bands of p62, HMW p62, and a strongly signalling non-specific band. Beta tubulin was used as a loading control.

The volcano plot comparing hFB treated with supernatant of KO sebocytes to WT sebocytes identified different cytokines that were upregulated. One such cytokine was the highly upregulated CXCL8 (Figure 6A).

We used the "Ingenuity Pathway Analysis" software (IPA, Quiagen) to investigate whether deregulation of gene groups could be used to predict the activation or inhibition of canonical signalling pathways. Pathway analysis revealed that the medium of the KO sebocytes induced genes in the pathogen-induced cytokine stromal signalling pathway network. The heatmap showed an upregulation of *CXCL8* and *IL1 beta* (Figure 6B). However, our attempt to confirm the sequencing results using qPCR (donors $n = 4$, technical triplicates) demonstrated a high variability of inflammatory responses depending on the FB donor. We identified a trend towards the induction of inflammatory chemokines (*CXCL8* and *IL1 beta*), but the regulation of *PTGS2* and *COL1A1* did not show a trend towards deregulation (Figure 6C). This prevented us from making a generalized interpretation of the inflammatory properties of the supernatant.

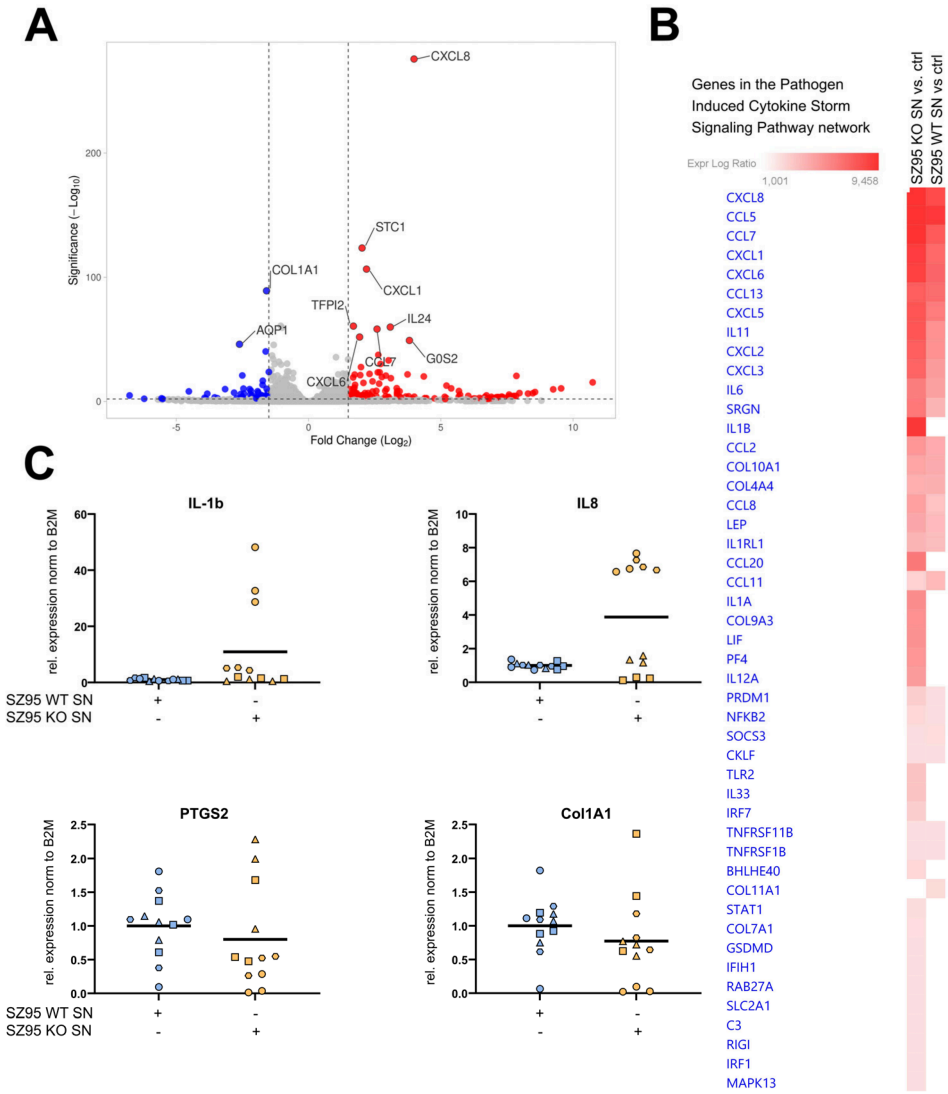

Figure 6. Exposure of hFB to supernatant (SN) of SZ95 WT and KO sebocytes results in increased cytokine expression. (**A**) Volcano blot of the RNA sequencing comparing hFB treated with KO sebocyte SN vs. hFB treated with WT sebocyte SN, with the FoldChange threshold of 1.8 and the significance threshold of $\log_{10}$ -2. Biological triplicates analyzed (**B**) Ingenuity Pathway Analysis (IPA) heatmap of Genes upregulated in Pathogen-Induced Cytokine Storm Signalling Pathway network. Comparison between hFB treated with KO supernatant vs. ctrl medium and hFB treated with SZ95 WT supernatant vs. ctrl medium. (**C**) qPCR gene deregulated as found in RNA sequencing volcano blots and IPA. Four hFB donors, Biological triplicates independently analyzed for each donor; symbols used for donor identification: ○ = m30y, Δ = m37y, □ = f41y, ⬡ = f23y.

4. Discussion

This study demonstrates that PPARγ has a significant impact on the lipid composition of SZ95 sebocytes at the cellular level. We detected an increased amount of oxidized lipid species in KO sebocytes. Furthermore, we observed striking differences in the amounts of native and high-molecular-weight p62 (a major cargo adaptor for macroautophagy) and an increase in LC3 total protein levels in KO sebocytes. We also observed an increased inflammatory response in hFB cells exposed to supernatant collected from SZ95 KO sebocytes, but this was only observed in cells from a subset of donors.

PPARγ has been reported to be involved in the differentiation of sebocytes and in lipid production [11]. Furthermore, activating PPARγ in SZ95 sebocytes reduced insulin-induced lipid synthesis and Akt/mTOR signalling [51]. In this study, we focused on the lipidome

during starvation as holocrine secretion is strongly associated with activated autophagy [4]. Our data revealed the deregulation of specific lipid classes in SZ95 sebocytes, a finding that had not been reported before. Moreover, our chosen mode of analysis resulted in a greater number of assigned lipid classes than previous studies on SZ95 sebocytes. We identified lipid classes with similar expression profiles to those previously reported (CE, DG, PC, PE, SM, TG) [52]. Another outcome of the untargeted LC-MS analysis was the significant shift in major lipid classes with ester-linked FAs towards lipids with ether-linked FAs in KO sebocytes, specifically PC O- and TG O- PCs are the most abundant structural phospholipid in mammalian cell membranes and make up the monolayer of lipid droplets [53,54]. TGs, which are neutral lipids confined primarily in the lipid droplet, are a highly efficient form of energy storage [55]. A shift towards ether phospholipids could influence the membrane stability, membrane-associated cellular processes, and energy storage, as ether lipids have previously been described as major structural components of cell membranes with the ability to reduce the membrane fluidity [56]. This effect on cellular processes was further corroborated by the results of the LION term analysis, which indicated an effect of the KO on cellular processes such as membrane trafficking, organelle formation, and receptor activation [57–60].

Another lipid class involved in cellular processes are FAs, which, besides their metabolic and structural function (as part of complex membrane lipids), can fulfil signalling functions both in native form [61] or upon transformation to eicosanoids in the wider sense [62]. We reported a shift towards very-long-chain FAs, which can possibly change the membrane permeability of the cell, which is especially important in the stratum corneum [63]. Furthermore, we observed a similar shift in the chain length of bound FAs in the lipid class level of PC O- and TG O-. It has been reported that PPARγ induces pathways to store long-chain FA as TG [64] and that FAs regulate PPARγ and thereby control lipid metabolism [65]. Therefore, the KO in SZ95 sebocytes could affect cellular signalling, lipid storage, and substrates for lipid signalling mediator synthesis.

The deregulation in lipid synthesis found in KO sebocytes might have further influence, as it has been described in SZ95 sebocytes that arachidonic acid and its keto-metabolites 5-KETE and 12-KETE regulate PPARγ signalling pathways, which in turn modulate phospholipid biosynthesis and induce neutral lipid synthesis [12]. Furthermore, it indicates oxidative stress within the cell upon the loss of PPARγ, which is in accordance with the proposed importance of the PPARγ system in regulating cellular responses to oxidative stress [66]. Another effect of the reduced levels of p62 and the disturbed autophagy could be the increase in ether lipids. Ether lipids are peroxisome-derived glycerophospholipids [56]. Peroxisome functionality is maintained through a specialized form of autophagy, called pexophagy, in which p62 is recognized to participate [67].

The increased cellular ROS that we observed here was likely due to mitochondrial damage. This is supported by the findings of a significant decrease in acylcarmine (CAR) levels, as a similar decrease in CAR had been described as an indicator of inhibited mitochondrial β-oxidation and mitochondrial dysfunction in mouse liver [68]. This increased cellular ROS usually goes hand in hand with oxidative modification of cellular biomolecules. We detected, with fluorescent probes and by MS, an elevation of oxidized lipids in the KO sebocytes. We have reported earlier that epithelial cells require functional macroautophagy to limit the accumulation of these potentially detrimental compounds, which are sequestered by the cargo adapter p62 and then degraded via the autophagosomal-lysosomal degradation pathway [8]. Therefore, it was surprising that the KO cells displayed no elevated p62, in either its native or HMW lipid-adducted form, in the basal state or upon stimulation with externally added excess oxidized lipids. Additionally, the total amount of LC3, the essential autophagy protein that upon lipidation (forming LC3 II out of LC3 I) incorporates into

the autophagosomal membrane, was elevated in the KOs. While some residual response to rapamycin, the standard autophagy agonist, and inhibition of LC3 lipidation by 3MA was visible in the immunoblots, the autophagic flux seems to be massively impaired by a combination of reduced p62 levels and impaired further processing of autophagosomes. Others [69] reported reduced autophagosome formation in p62-depleted HeLa cells, specifically a decreased LC3 assembly, which could explain the increased LC3 levels we detected in KO sebocytes. Of note, p62 is also required for the assembly of inclusion bodies that sequester and partially detoxify an excess of reactive compounds when they cannot be processed by proteolytic or autophagic pathways, and the IF staining shows that these are strongly reduced in size and number in the KO cells. A lack of the ability to sequester the reactive lipids could, together with elevated ROS generation due to mitochondrial damage [20] also contribute to their elevated levels we detected in the lipid extracts and by fluorescent sensors in these cells and promote an inflammatory state [8] (Figure 4). The role of dermal fibroblasts as signal relays in inflammatory skin diseases is a novel concept recently reported [13], and we chose to investigate whether the mediators released by sebocytes would affect fibroblast fate, a mechanism that could be important for skin inflammation driven by the sebaceous glands. The supernatant we collected from SZ95 KO sebocytes had a pro-inflammatory function in different hFB donors and generated increased *IL-1 beta* and *IL-8* levels. The response in this exploratory study was, however, absent in part of the donors; thus, a general interpretation requires further experimentation. As oxidized lipids can function as inflammatory mediators [49] and sebum can influence immune cells and the connective tissue [70], one possible explanation might be the increased oxidative lipid species contained in the KO sebocytes. These KO sebocytes might have a deregulated secretome, which can influence other dermal cells, similar to how the deregulation of IL-1 alpha in KCs influences the inflammatory cytokines in fibroblasts [71]. Another role in the increased inflammation signalling in the hFB might be the disturbed autophagy in KO sebocytes. KC autophagy has previously been shown to dampen skin inflammation and tumorigenesis [50], and as KCs and sebocytes develop from the same ancestor stem cell [2], they might similarly influence the dermal compartment.

5. Conclusions

In conclusion, the loss of PPARγ in SZ95 sebocytes altered the lipidome and epilipidome of these cells at the stages of synthesis, oxidation, signalling, and degradation. This is likely promoted by a massive impairment of the autophagic adaptor machinery through dysregulation of p62/SQSTM-1, which suggests the importance of PPARγ in regulating cutaneous lipid metabolism and lipid-mediated inflammation.

Author Contributions: Conceptualization, D.T., F.G.; Data curation, A.S.; Formal analysis, A.S., M.S., C.K., S.J., D.K., K.L. and M.M.; Funding acquisition, F.G. and D.T.; Investigation, A.S., M.S., I.-M.N., E.C. and M.M.; Methodology, I.-M.N., E.C. and C.K.; Project administration, F.G. and A.S.; Resources, I.-M.N.; Software, C.B. and C.K.; Supervision. F.G., D.T. and E.C.; Validation, F.G., D.T. and E.C.; Visualization, A.S., C.K. and C.B.; Writing—original draft, A.S., F.G. and D.T.; Writing—review & editing, F.G., C.C.Z. and D.T. All authors have read and agreed to the published version of the manuscript.

Funding: This research was funded in part by the Austrian Science Fund (FWF) [grant I-5627 B]. For open access purposes, the author has applied a CC BY public copyright license to any author accepted manuscript version arising from this submission. D.T. was supported by the Hungarian National Research, Development and Innovation Office FK-132296 and ANN 139589. C.B., S.J, and C.K. were supported by the contribution of the Federal Ministry of Economy, Energy and Tourism of Austria and the National Foundation for Research, Technology, and Development of Austria to the Christian Doppler Laboratory for Skin Multimodal Imaging of Aging and Senescence (SKINMAGINE).

Data Availability Statement: The data presented in this study are available on request from the corresponding author as there is no repository for non-standardized epilipidomic data.

Acknowledgments: We acknowledge the support of the EMBL Metabolomics Core Facility (MCF) in the acquisition and analysis of liquid chromatography-mass spectrometry data and the support by Wolfgang Bicker from FTC Forensisch-Toxikologisches Labor Betriebs gmbH. We acknowledge the support of the Core Facilities of the Medical University of Vienna, a member of VLSI, in the acquisition and analysis of bulk-RNA-seq data. The imaging core faculty of the MUW is acknowledged for assistance in imaging. F.G. gratefully acknowledges the financial support of the Federal Ministry of Economy, Energy and Tourism of Austria and the National Foundation for Research, Technology, and Development of Austria and of Chanel PB to the Christian Doppler Laboratory for Skin Multimodal Imaging of Aging and Senescence.

Conflicts of Interest: The authors declare no conflicts of interest.

Abbreviations

3MA	3-Methyladenine
BHT	Butylhydroxytoluol
BioPan	Bioinformatics Methodology For Pathway Analysis
CAR	Acylcarmine
DG	Diacylglycerols
dhCer	Dihydroceramide
dhSM	dihydrosphingomyelins
EGF	Epidermal growth factor
FA	Fatty Acids
hFB	Human Fibroblasts
HMW	High-molecular-weight
IPA	Ingenuity Pathway Analysis
KC	Keratinocyte
KO	Knockout
LION	Lipid Ontology
LPS	Lyso-PS
MS	Mass Spectrometry
OxPAPC	Oxidized Phospholipids
PAPC	1-Palmitoyl-2-arachidonoyl-sn-glycero-3-PC
PC	phosphatidylcholines
PC O-	ether-phosphatidylcholines
PE	phosphatidylethanolamines
PI	phosphatidylinositol
PONPC	1-palmitoyl-2-(9-oxo)nonanoyl-sn-glycero-3-phosphocholine
POVPC	1-palmitoyl-2-(5-oxovaleroyl)-sn-glycero-3-phosphocholine
PPARγ	Peroxisome Proliferator-Activated Receptor gamma
PS	phosphatidylserine
RAPA	Rapamycin
ROS	Reactive oxygen species
SG	Sebaceous Gland
SM	Sphingomyelin
TG	Triglycerides
TG O-	Alkyl-triglycerides
WT	wildtype

Appendix A

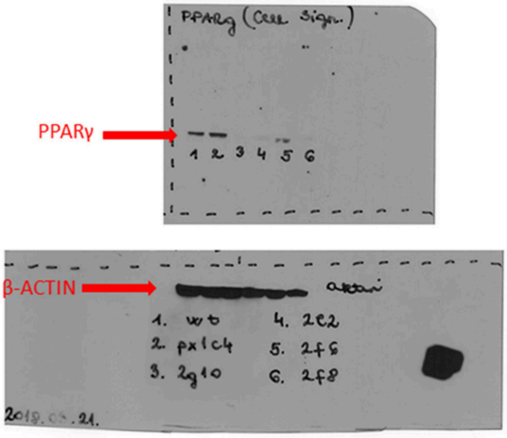

Figure A1. Confirmation of PPARγ knockout in SZ95 sebocytes. Four different clones were generated containing the PPARγ knockout. Lanes from left to right: 1 = wildtype, 2 = clone px1c4, 3 = clone 2g10 (used in further experimentation), 4 = clone 2e2, 5 = clone 2f6, 6 = clone 2f8. The top panel shows the PPARγ immunoblot, and the bottom panel the loading control b-actin immunoblot.

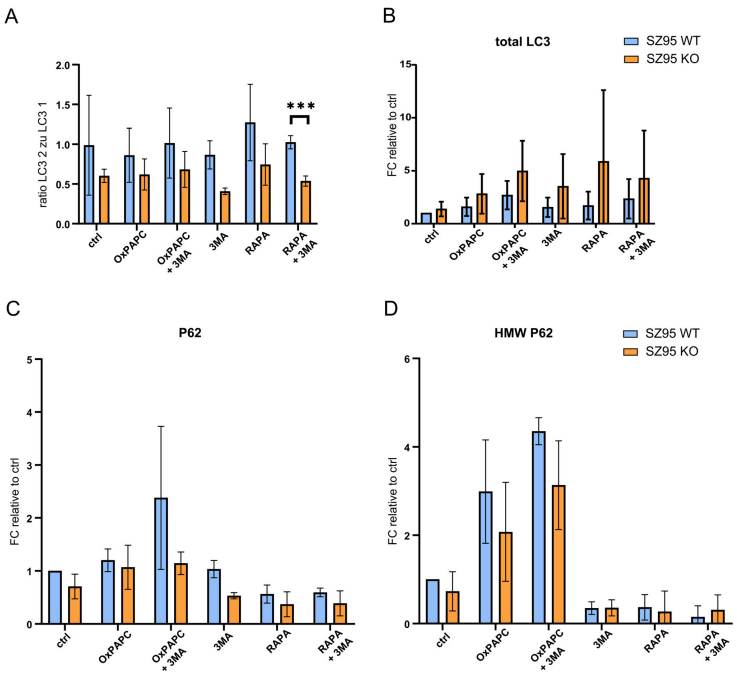

Figure A2. Measurement of protein expression in WT and KO sebocytes upon activation and inhibition of autophagy. (**A**) LC3 I and LC3 II expression was evaluated after 4 h of treatment by measuring the volume of the corresponding band in Image Lab. Background was subtracted, and volume was normalized to Tubulin. Ratio of LC3 II/I expression was calculated. Biological triplicates were independently analyzed for each cell type, *t*-Test, *** < 0.005. (**B**) Total amount of LC3 was calculated by combining the measured amount of LC3 I and LC3 II after subtracting the background and normalizing to Tubulin. Data was normalized to SZ95 WT ctrl. Biological triplicates independently analyzed for each cell type (**C**) p62 expression was evaluated after 24 h of treatment by measuring the volume of the corresponding band in Image Lab. Background was subtracted, and volume was normalized to Tubulin. Expression was normalized to SZ95 WT ctrl. Biological triplicates independently analyzed for each cell type. (**D**) HMW p62 expression was evaluated after 24 h of treatment by measuring the volume of the corresponding band in Image Lab. Background was subtracted and volume was normalized to Tubulin. Expression was normalized to SZ95 WT ctrl. Biological triplicates independently analyzed for each cell type.

References

1. Düz, T.; Torocsik, D.; Simmering, A.; Wolf, P.; Gallinat, S.; Baumbach, J.; Holzscheck, N. High-Resolution Spatial Map of the Human Facial Sebaceous Gland Reveals Marker Genes and Decodes Sebocyte Differentiation. *J. Investig. Dermatol.* **2025**, *146*, 40–54. [CrossRef]
2. Schneider, M.R. Lipid droplets and associated proteins in sebocytes. *Exp. Cell Res.* **2016**, *340*, 205–208. [CrossRef]
3. Zouboulis, C.C.; Baron, J.M.; Böhm, M.; Kippenberger, S.; Kurzen, H.; Reichrath, J.; Thielitz, A. Frontiers in sebaceous gland biology and pathology. *Exp. Dermatol.* **2008**, *17*, 542–551. [CrossRef] [PubMed]
4. Seo, S.H.; Jung, J.Y.; Park, K.; Hossini, A.M.; Zouboulis, C.C.; Lee, S.E. Autophagy regulates lipid production and contributes to the sebosuppressive effect of retinoic acid in human SZ95 sebocytes. *J. Dermatol. Sci.* **2020**, *98*, 128–136. [CrossRef] [PubMed]
5. Fischer, H.; Fumicz, J.; Rossiter, H.; Napirei, M.; Buchberger, M.; Tschachler, E.; Eckhart, L. Holocrine Secretion of Sebum Is a Unique DNase2-Dependent Mode of Programmed Cell Death. *J. Investig. Dermatol.* **2017**, *137*, 587–594. [CrossRef]
6. Hossini, A.M.; Hou, X.; Exner, T.; Fauler, B.; Eberle, J.; Rabien, A.; Makrantonaki, E.; Zouboulis, C.C. Free Fatty Acids Induce Lipid Accumulation, Autophagy, and Apoptosis in Human Sebocytes. *Skin Pharmacol. Physiol.* **2023**, *36*, 1–15. [CrossRef]
7. Rossiter, H.; Copic, D.; Direder, M.; Gruber, F.; Zoratto, S.; Marchetti-Deschmann, M.; Kremslehner, C.; Sochorová, M.; Nagelreiter, I.-M.; Mlitz, V.; et al. Autophagy protects murine preputial glands against premature aging, and controls their sebum phospholipid and pheromone profile. *Autophagy* **2022**, *18*, 1005–1019. [CrossRef]
8. Zhao, Y.; Zhang, C.-F.; Rossiter, H.; Eckhart, L.; König, U.; Karner, S.; Mildner, M.; Bochkov, V.N.; Tschachler, E.; Gruber, F. Autophagy is induced by UVA and promotes removal of oxidized phospholipids and protein aggregates in epidermal keratinocytes. *J. Investig. Dermatol.* **2013**, *133*, 1629–1637. [CrossRef] [PubMed]
9. Song, X.; Narzt, M.S.; Nagelreiter, I.M.; Hohensinner, P.; Terlecki-Zaniewicz, L.; Tschachler, E.; Grillari, J.; Gruber, F. Autophagy deficient keratinocytes display increased DNA damage, senescence and aberrant lipid composition after oxidative stress in vitro and in vivo. *Redox Biol.* **2017**, *11*, 219–230. [CrossRef]
10. Rossiter, H.; Stübiger, G.; Gröger, M.; König, U.; Gruber, F.; Sukseree, S.; Mlitz, V.; Buchberger, M.; Oskolkova, O.; Bochkov, V.; et al. Inactivation of autophagy leads to changes in sebaceous gland morphology and function. *Exp. Dermatol.* **2018**, *27*, 1142–1151. [CrossRef]
11. Briganti, S.; Mosca, S.; Di Nardo, A.; Flori, E.; Ottaviani, M. New Insights into the Role of PPARγ in Skin Physiopathology. *Biomolecules* **2024**, *14*, 728. [CrossRef]
12. Dozsa, A.; Dezso, B.; Toth, B.I.; Bacsi, A.; Poliska, S.; Camera, E.; Picardo, M.; Zouboulis, C.C.; Bíró, T.; Schmitz, G.; et al. PPARγ-mediated and arachidonic acid-dependent signaling is involved in differentiation and lipid production of human sebocytes. *J. Investig. Dermatol.* **2014**, *134*, 910–920. [CrossRef] [PubMed]
13. Numata, T.; Shia, M.; Nakamura, Y.; Li, F.; Chan, H.; Nakatsuji, T.; Cavagnero, K.J.; Simmons, J.; Li, H.; Joshi, A.A.; et al. Dermal fibroblasts respond to IL-4 and IL-13 and promote T cell recruitment in atopic dermatitis. *J. Clin. Investig.* **2026**, *136*, e196108. [CrossRef]
14. Davies, S.S.; Pontsler, A.V.; Marathe, G.K.; Harrison, K.A.; Murphy, R.C.; Hinshaw, J.C.; Prestwich, G.D.; Hilaire, A.S.; Prescott, S.M.; Zimmerman, G.A.; et al. Oxidized alkyl phospholipids are specific, high affinity peroxisome proliferator-activated receptor γ ligands and agonists. *J. Biol. Chem.* **2001**, *276*, 16015–16023. [CrossRef] [PubMed]
15. Leitinger, N. Oxidized phospholipids as modulators of inflammation in atherosclerosis. *Curr. Opin. Lipidol.* **2003**, *14*, 421–430. [CrossRef] [PubMed]
16. Faghfouri, A.H.; Khajebishak, Y.; Payahoo, L.; Faghfuri, E.; Alivand, M. PPAR-gamma agonists: Potential modulators of autophagy in obesity. *Eur. J. Pharmacol.* **2021**, *912*, 174562. [CrossRef]
17. Kiani, P.; Khodadadi, E.S.; Nikdasti, A.; Yarahmadi, S.; Gheibi, M.; Yousefi, Z.; Ehtiati, S.; Yahyazadeh, S.; Shafiee, S.M.; Taghizadeh, M.; et al. Autophagy and the peroxisome proliferator-activated receptor signaling pathway: A molecular ballet in lipid metabolism and homeostasis. *Mol. Cell. Biochem.* **2025**, *480*, 3477–3499. [CrossRef] [PubMed]
18. Wei, Y.; Zou, Z.; Becker, N.; Anderson, M.; Sumpter, R.; Xiao, G.; Kinch, L.; Koduru, P.; Christudass, C.S.; Veltri, R.W.; et al. EGFR-mediated Beclin 1 phosphorylation in autophagy suppression, tumor progression, and tumor chemoresistance. *Cell* **2013**, *154*, 1269–1284. [CrossRef]
19. Zouboulis, C.C.; Seltmann, H.; Orfanos, C.E.; Neitzel, H. Establishment and Characterization of an Immortalized Human Sebaceous Gland Cell Line (SZ95)1. *J. Investig. Dermatol.* **1999**, *113*, 1011–1020. [CrossRef] [PubMed]
20. Lénárt, K.; Kovács, D.; Demeny, M.; Ujlaki, G.; Baran, S.; Kókai, E.; Póliska, S.; Bacsó, Z.J.; Banko, C.; Zouboulis, C.C.; et al. PPARγ Deficiency Impairs Lipid Metabolism and Mitochondrial Homeostasis in SZ95 Sebocytes. *bioRxiv*, 2026; *manuscript submitted for publication*.
21. Narzt, M.-S.; Nagelreiter, I.-M.; Oskolkova, O.; Bochkov, V.N.; Latreille, J.; Fedorova, M.; Ni, Z.; Sialana, F.J.; Lubec, G.; Filzwieser, M.; et al. A novel role for NUPR1 in the keratinocyte stress response to UV oxidized phospholipids. *Redox Biol.* **2019**, *20*, 467–482. [CrossRef]

22. Gruber, F.; Bicker, W.; Oskolkova, O.V.; Tschachler, E.; Bochkov, V.N. A simplified procedure for semi-targeted lipidomic analysis of oxidized phosphatidylcholines induced by UVA irradiation. *J. Lipid Res.* **2012**, *53*, 1232–1242. [CrossRef] [PubMed]
23. Tsugawa, H.; Cajka, T.; Kind, T.; Ma, Y.; Higgins, B.; Ikeda, K.; Kanazawa, M.; VanderGheynst, J.; Fiehn, O.; Arita, M. MS-DIAL: Data-independent MS/MS deconvolution for comprehensive metabolome analysis. *Nat. Methods* **2015**, *12*, 523–526. [CrossRef]
24. Drotleff, B.; Lämmerhofer, M. Guidelines for Selection of Internal Standard-Based Normalization Strategies in Untargeted Lipidomic Profiling by LC-HR-MS/MS. *Anal. Chem.* **2019**, *91*, 9836–9843. [CrossRef]
25. Drotleff, B.; Roth, S.R.; Henkel, K.; Calderón, C.; Schlotterbeck, J.; Neukamm, M.A.; Lämmerhofer, M. Lipidomic profiling of non-mineralized dental plaque and biofilm by untargeted UHPLC-QTOF-MS/MS and SWATH acquisition. *Anal. Bioanal. Chem.* **2020**, *412*, 2303–2314. [CrossRef]
26. Gaud, C.; Sousa, B.C.; Nguyen, A.; Fedorova, M.; Ni, Z.; O'Donnell, V.B.; Wakelam, M.J.O.; Andrews, S.; Lopez-Clavijo, A.F. BioPAN: A web-based tool to explore mammalian lipidome metabolic pathways on LIPID MAPS. *F1000Research* **2021**, *10*, 4. [CrossRef]
27. Molenaar, M.R.; Jeucken, A.; Wassenaar, T.A.; Van De Lest, C.H.A.; Brouwers, J.F.; Helms, J.B. LION/web: A web-based ontology enrichment tool for lipidomic data analysis. *GigaScience* **2019**, *8*, giz061. [CrossRef] [PubMed]
28. Molenaar, M.R.; Haaker, M.W.; Vaandrager, A.B.; Houweling, M.; Helms, J.B. Lipidomic profiling of rat hepatic stellate cells during activation reveals a two-stage process accompanied by increased levels of lysosomal lipids. *J. Biol. Chem.* **2023**, *299*, 103042. [CrossRef]
29. Benjamini, Y.; Hochberg, Y. Controlling the False Discovery Rate: A Practical and Powerful Approach to Multiple Testing. *J. R. Stat. Soc. Ser. B Methodol.* **1995**, *57*, 289–300. [CrossRef]
30. Sochorová, M.; Kremslehner, C.; Nagelreiter, I.-M.; Ferrara, F.; Lisicin, M.M.; Narzt, M.-S.; Bauer, C.; Stiegler, A.; Golabi, B.; Vávrová, K.; et al. Deletion of NRF2 disturbs composition, morphology, and differentiation of the murine tail epidermis in chronological aging. *BioFactors* **2023**, *49*, 684–698. [CrossRef]
31. Berliner, J.A.; Subbanagounder, G.; Leitinger, N.; Watson, A.D.; Vora, D. Evidence for a role of phospholipid oxidation products in atherogenesis. *Trends Cardiovasc. Med.* **2001**, *11*, 142–147. [CrossRef]
32. Martin, M. Cutadapt removes adapter sequences from high-throughput sequencing reads. *EMBnet J.* **2011**, *17*, 10–12. [CrossRef]
33. NCBI. GRCh38 Human Reference Genome. Available online: https://ftp.ncbi.nlm.nih.gov/genomes/all/GCA/000/001/405/GCA_000001405.15_GRCh38/seqs_for_alignment_pipelines.ucsc_ids/GCA_000001405.15_GRCh38_no_alt_analysis_set.fna.gz (accessed on 27 September 2018).
34. Gencode. Human Genome Annotations. Available online: https://ftp.ebi.ac.uk/pub/databases/gencode/Gencode_human/release_29/gencode.v29.chr_patch_hapl_scaff.annotation.gtf.gz (accessed on 22 November 2018).
35. Dobin, A.; Davis, C.A.; Schlesinger, F.; Drenkow, J.; Zaleski, C.; Jha, S.; Batut, P.; Chaisson, M.; Gingeras, T.R. STAR: Ultrafast universal RNA-seq aligner. *Bioinformatics* **2013**, *29*, 15–21. [CrossRef]
36. Love, M.I.; Huber, W.; Anders, S. Moderated estimation of fold change and dispersion for RNA-seq data with DESeq2. *Genome Biol.* **2014**, *15*, 550. [CrossRef]
37. Goedhart, J.; Luijsterburg, M.S. VolcaNoseR is a web app for creating, exploring, labeling and sharing volcano plots. *Sci. Rep.* **2020**, *10*, 20560. [CrossRef]
38. Gruber, F.; Mayer, H.; Lengauer, B.; Mlitz, V.; Sanders, J.M.; Kadl, A.; Bilban, M.; de Martin, R.; Wagner, O.; Kensler, T.W.; et al. NF-E2-related factor 2 regulates the stress response to UVA-1-oxidized phospholipids in skin cells. *FASEB J.* **2010**, *24*, 39–48. [CrossRef]
39. Pfaffl, M.W. A new mathematical model for relative quantification in real-time RT–PCR. *Nucleic Acids Res.* **2001**, *29*, e45. [CrossRef]
40. Fay, M.P.; Proschan, M.A. Wilcoxon-Mann-Whitney or *t*-test? On assumptions for hypothesis tests and multiple interpretations of decision rules. *Stat. Surv.* **2010**, *4*, 1–39. [CrossRef] [PubMed]
41. Karvelis, P.; Oyvindlr. *povilaskarvelis/DataViz*, v3.2.4.; Zenodo: Geneva, Switzerland, 2024. [CrossRef]
42. Campbell, R. raacampbell/sigstar. MATLAB. 2024. Available online: https://github.com/raacampbell/sigstar (accessed on 24 March 2025).
43. Lum, J.J.; Bauer, D.E.; Kong, M.; Harris, M.H.; Li, C.; Lindsten, T.; Thompson, C.B. Growth Factor Regulation of Autophagy and Cell Survival in the Absence of Apoptosis. *Cell* **2005**, *120*, 237–248. [CrossRef]
44. Chen, Z.; Ho, I.-L.; Soeung, M.; Yen, E.-Y.; Liu, J.; Yan, L.; Rose, J.L.; Srinivasan, S.; Jiang, S.; Edward Chang, Q.; et al. Ether phospholipids are required for mitochondrial reactive oxygen species homeostasis. *Nat. Commun.* **2023**, *14*, 2194. [CrossRef] [PubMed]
45. Forman, H.J.; Augusto, O.; Brigelius-Flohe, R.; Dennery, P.A.; Kalyanaraman, B.; Ischiropoulos, H.; Mann, G.E.; Radi, R.; Roberts, L.J.; Vina, J.; et al. Even free radicals should follow some rules: A guide to free radical research terminology and methodology. *Free Radic. Biol. Med.* **2015**, *78*, 233–235. [CrossRef] [PubMed]

46. Bochkov, V.N.; Oskolkova, O.V.; Birukov, K.G.; Levonen, A.-L.; Binder, C.J.; Stöckl, J. Generation and biological activities of oxidized phospholipids. *Antioxid. Redox Signal.* **2010**, *12*, 1009–1059. [CrossRef]
47. Li Pomi, F.; Gammeri, L.; Borgia, F.; Di Gioacchino, M.; Gangemi, S. Oxidative Stress and Skin Diseases: The Role of Lipid Peroxidation. *Antioxidants* **2025**, *14*, 555. [CrossRef]
48. Jiang, M.; Fernandez, S.; Jerome, W.G.; He, Y.; Yu, X.; Cai, H.; Boone, B.; Yi, Y.; Magnuson, M.A.; Roy-Burman, P.; et al. Disruption of PPARγ signaling results in mouse prostatic intraepithelial neoplasia involving active autophagy. *Cell Death Differ.* **2010**, *17*, 469–481. [CrossRef] [PubMed]
49. Yeh, M.; Leitinger, N.; de Martin, R.; Onai, N.; Matsushima, K.; Vora, D.K.; Berliner, J.A.; Reddy, S.T. Increased Transcription of IL-8 in Endothelial Cells Is Differentially Regulated by TNF-α and Oxidized Phospholipids. *Arterioscler. Thromb. Vasc. Biol.* **2001**, *21*, 1585–1591. [CrossRef] [PubMed]
50. Van Hove, L.; Toniolo, A.; Ghiasloo, M.; Lecomte, K.; Boone, F.; Ciers, M.; Raaijmakers, K.; Vandamme, N.; Roels, J.; Maschalidi, S.; et al. Autophagy critically controls skin inflammation and apoptosis-induced stem cell activation. *Autophagy* **2023**, *19*, 2958–2971. [CrossRef]
51. Mastrofrancesco, A.; Ottaviani, M.; Cardinali, G.; Flori, E.; Briganti, S.; Ludovici, M.; Zouboulis, C.C.; Lora, V.; Camera, E.; Picardo, M. Pharmacological PPARγ modulation regulates sebogenesis and inflammation in SZ95 human sebocytes. *Biochem. Pharmacol.* **2017**, *138*, 96–106. [CrossRef]
52. Kovács, D.; Camera, E.; Póliska, S.; Cavallo, A.; Maiellaro, M.; Dull, K.; Gruber, F.; Zouboulis, C.C.; Szegedi, A.; Törőcsik, D. Linoleic Acid Induced Changes in SZ95 Sebocytes—Comparison with Palmitic Acid and Arachidonic Acid. *Nutrients* **2023**, *15*, 3315. [CrossRef]
53. Moessinger, C.; Klizaite, K.; Steinhagen, A.; Philippou-Massier, J.; Shevchenko, A.; Hoch, M.; Ejsing, C.S.; Thiele, C. Two different pathways of phosphatidylcholine synthesis, the Kennedy Pathway and the Lands Cycle, differentially regulate cellular triacylglycerol storage. *BMC Cell Biol.* **2014**, *15*, 43. [CrossRef]
54. Wang, B.; Tontonoz, P. Phospholipid Remodeling in Physiology and Disease. *Annu. Rev. Physiol.* **2019**, *81*, 165–188. [CrossRef]
55. Walther, T.C.; Farese, R.V. Lipid Droplets and Cellular Lipid Metabolism. *Annu. Rev. Biochem.* **2012**, *81*, 687–714. [CrossRef]
56. Dean, J.M.; Lodhi, I.J. Structural and functional roles of ether lipids. *Protein Cell* **2018**, *9*, 196–206. [CrossRef]
57. Frallicciardi, J.; Melcr, J.; Siginou, P.; Marrink, S.J.; Poolman, B. Membrane thickness, lipid phase and sterol type are determining factors in the permeability of membranes to small solutes. *Nat. Commun.* **2022**, *13*, 1605. [CrossRef]
58. Kaltenegger, M.; Kremser, J.; Frewein, M.P.K.; Ziherl, P.; Bonthuis, D.J.; Pabst, G. Intrinsic lipid curvatures of mammalian plasma membrane outer leaflet lipids and ceramides. *Biochim. Biophys. Acta BBA—Biomembr.* **2021**, *1863*, 183709. [CrossRef]
59. Mužić, T.; Tounsi, F.; Madsen, S.B.; Pollakowski, D.; Konrad, M.; Heimburg, T. Melting transitions in biomembranes. *Biochim. Biophys. Acta BBA—Biomembr.* **2019**, *1861*, 183026. [CrossRef] [PubMed]
60. Sharma, V.K.; Srinivasan, H.; Gupta, J.; Mitra, S. Lipid lateral diffusion: Mechanisms and modulators. *Soft Matter* **2024**, *20*, 7763–7796. [CrossRef]
61. Milligan, G.; Stoddart, L.A.; Brown, A.J. G protein-coupled receptors for free fatty acids. *Cell. Signal.* **2006**, *18*, 1360–1365. [CrossRef] [PubMed]
62. Biernacki, M.; Skrzydlewska, E. Metabolic pathways of eicosanoids—Derivatives of arachidonic acid and their significance in skin. *Cell. Mol. Biol. Lett.* **2025**, *30*, 7. [CrossRef]
63. Zwara, A.; Wertheim-Tysarowska, K.; Mika, A. Alterations of Ultra Long-Chain Fatty Acids in Hereditary Skin Diseases—Review Article. *Front. Med.* **2021**, *8*, 730855. [CrossRef] [PubMed]
64. Nakamura, M.T.; Yudell, B.E.; Loor, J.J. Regulation of energy metabolism by long-chain fatty acids. *Prog. Lipid Res.* **2014**, *53*, 124–144. [CrossRef]
65. Varga, T.; Czimmerer, Z.; Nagy, L. PPARs are a unique set of fatty acid regulated transcription factors controlling both lipid metabolism and inflammation. *Biochim. Biophys. Acta BBA—Mol. Basis Dis.* **2011**, *1812*, 1007–1022. [CrossRef] [PubMed]
66. Zhang, Q.; Seltmann, H.; Zouboulis, C.C.; Travers, J.B. Activation of platelet-activating factor receptor in SZ95 sebocytes results in inflammatory cytokine and prostaglandin E2 production. *Exp. Dermatol.* **2006**, *15*, 769–774. [CrossRef] [PubMed]
67. Li, H.; Lismont, C.; Revenco, I.; Hussein, M.A.F.; Costa, C.F.; Fransen, M. The Peroxisome-Autophagy Redox Connection: A Double-Edged Sword? *Front. Cell Dev. Biol.* **2021**, *9*, 814047. [CrossRef] [PubMed]
68. Bjørndal, B.; Alterås, E.K.; Lindquist, C.; Svardal, A.; Skorve, J.; Berge, R.K. Associations between fatty acid oxidation, hepatic mitochondrial function, and plasma acylcarnitine levels in mice. *Nutr. Metab.* **2018**, *15*, 10. [CrossRef]
69. Tsuchiya, M.; Ogawa, H.; Koujin, T.; Kobayashi, S.; Mori, C.; Hiraoka, Y.; Haraguchi, T. Depletion of autophagy receptor p62/SQSTM1 enhances the efficiency of gene delivery in mammalian cells. *FEBS Lett.* **2016**, *590*, 2671–2680. [CrossRef]

70. Zouboulis, C.C.; Coenye, T.; He, L.; Kabashima, K.; Kobayashi, T.; Niemann, C.; Nomura, T.; Oláh, A.; Picardo, M.; Quist, S.R.; et al. Sebaceous immunobiology—Skin homeostasis, pathophysiology, coordination of innate immunity and inflammatory response and disease associations. *Front. Immunol.* **2022**, *13*, 1029818. [CrossRef]
71. Russo, B.; Brembilla, N.C.; Chizzolini, C. Interplay Between Keratinocytes and Fibroblasts: A Systematic Review Providing a New Angle for Understanding Skin Fibrotic Disorders. *Front. Immunol.* **2020**, *11*, 648. [CrossRef]